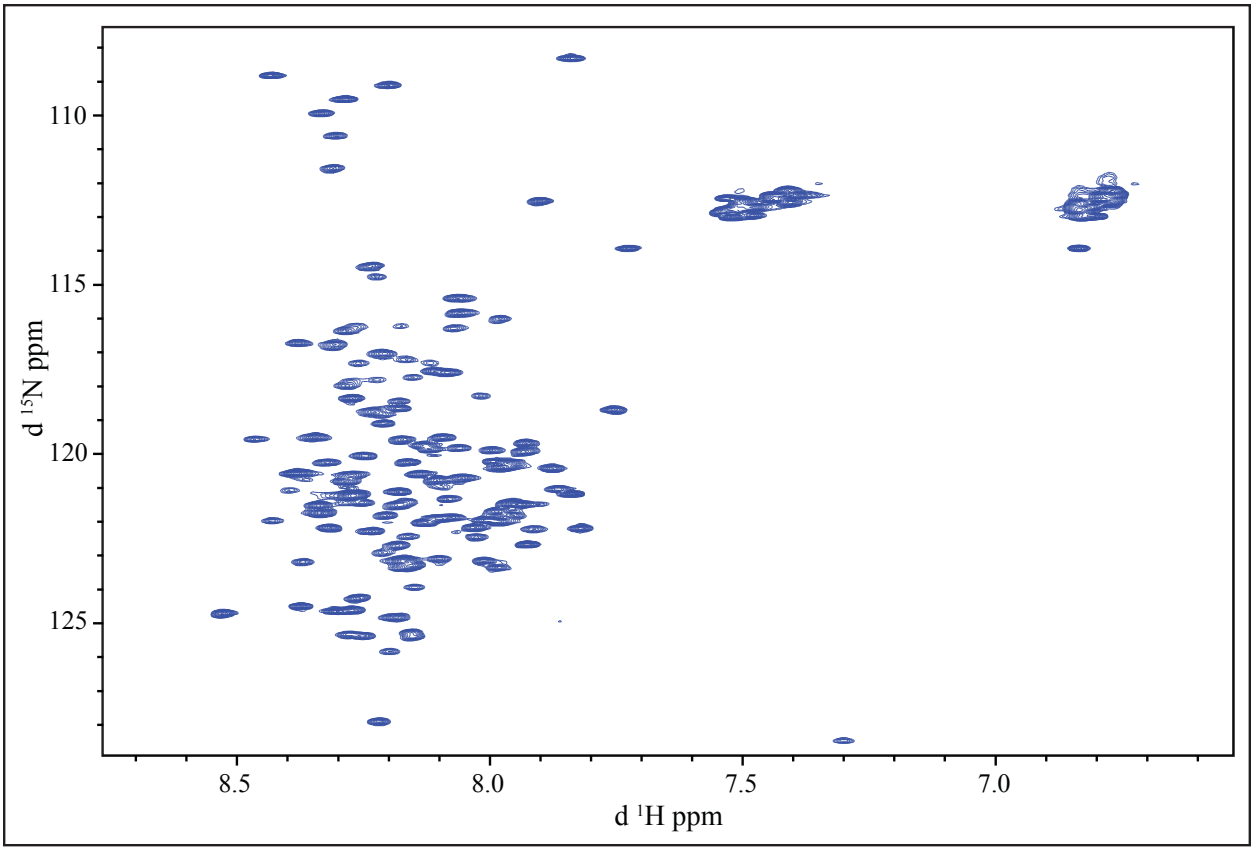

Figure S1. The 2D ^{1}H-^{15}N HSQC spectra of Atg13[571-700]. The lack of dispersion in the amide region of the spectrum is indicative that this region is intrinsically disordered. Related to Fig. 1.

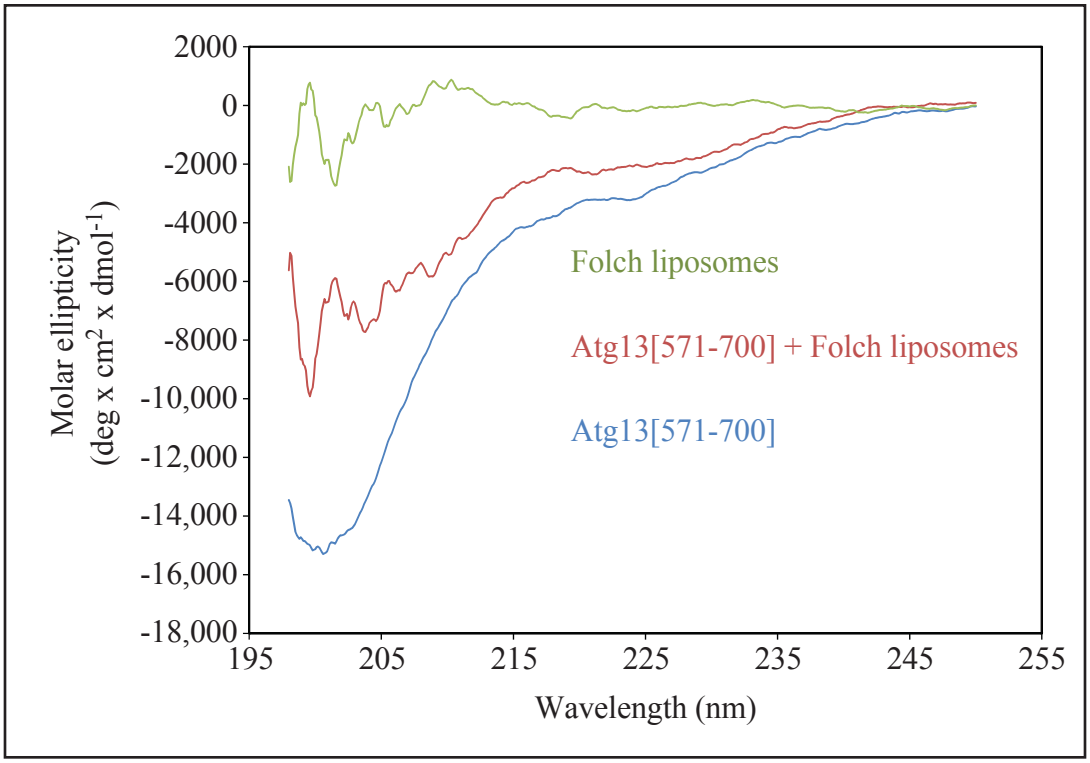

Figure S2. Circular dichroism spectroscopy on Atg13[571-700] (blue), Folch liposomes (green) and Atg13[571-700] with liposomes (red) in 200 mM NaCl. No increase in CD signal was observed at 222 nm indicating that Atg13[571-700] does not gain helical content upon binding to liposomes. Related to Fig. 1.

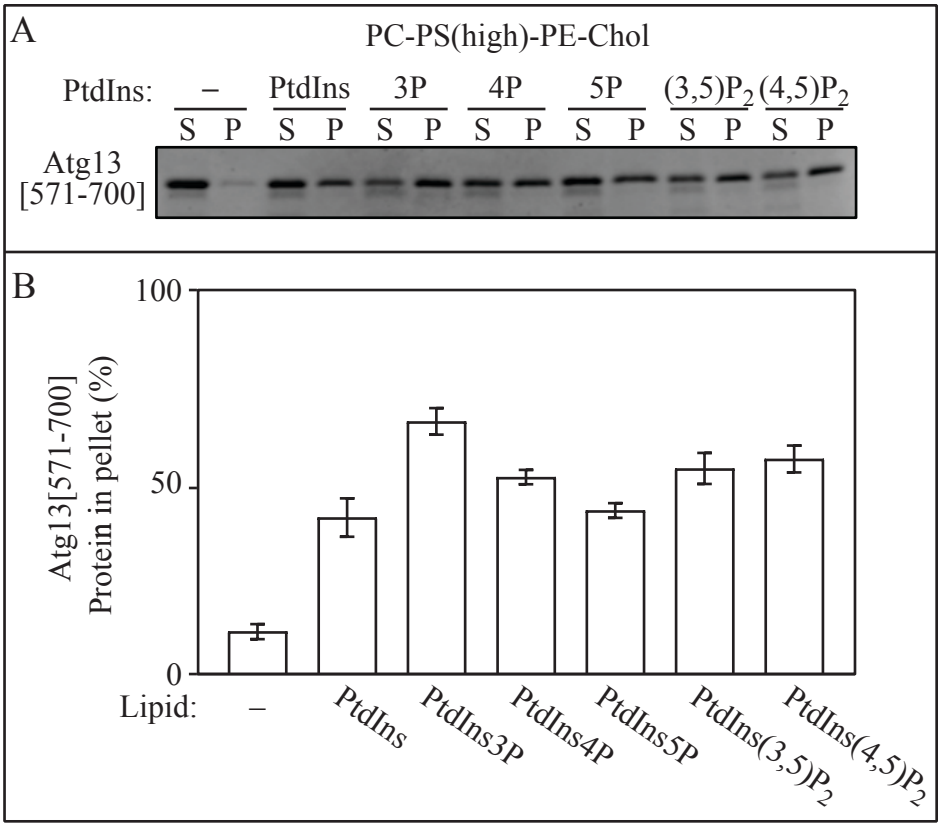

Figure S3. Atg13[571-700] has little preference for different phosphoinositides. Liposome sedimentation was performed with Atg13[571-700] and liposomes composed of PC, PS, PE, cholesterol and different phosphorylated PtdIns. Quantification of the densitometry is shown with error bars representing the SD from 3 experiments.

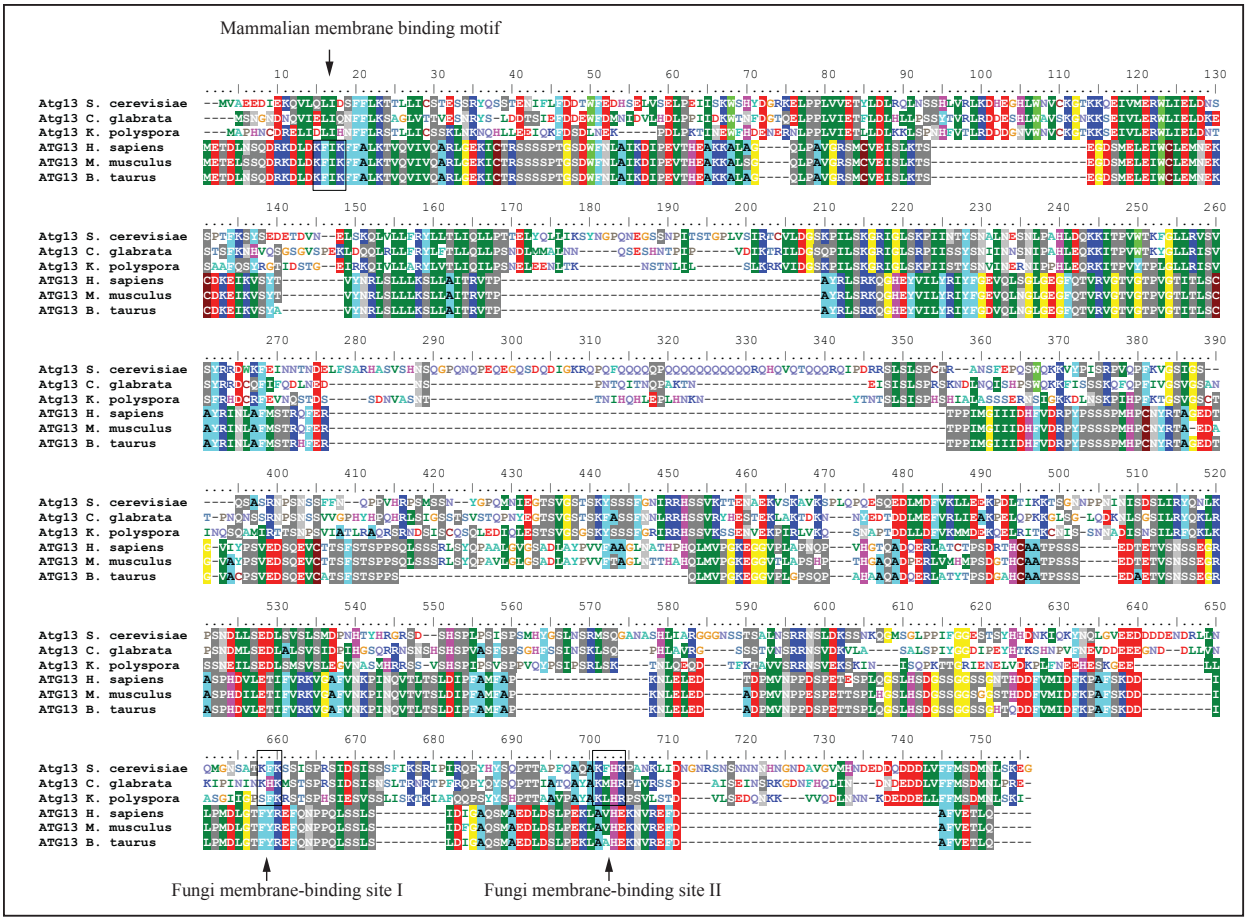

Figure S4. Amino acid sequence alignment of Atg13 from fungi and ATG13 from mammals. The previously reported phospholipid-binding motif in mammalian proteins and 2 sites in fungal proteins identified in this study are highlighted by gray rectangles. Alignment was created in the BioEdit Sequence Alignment Editor [33]. Related to Figure 1 and 2.

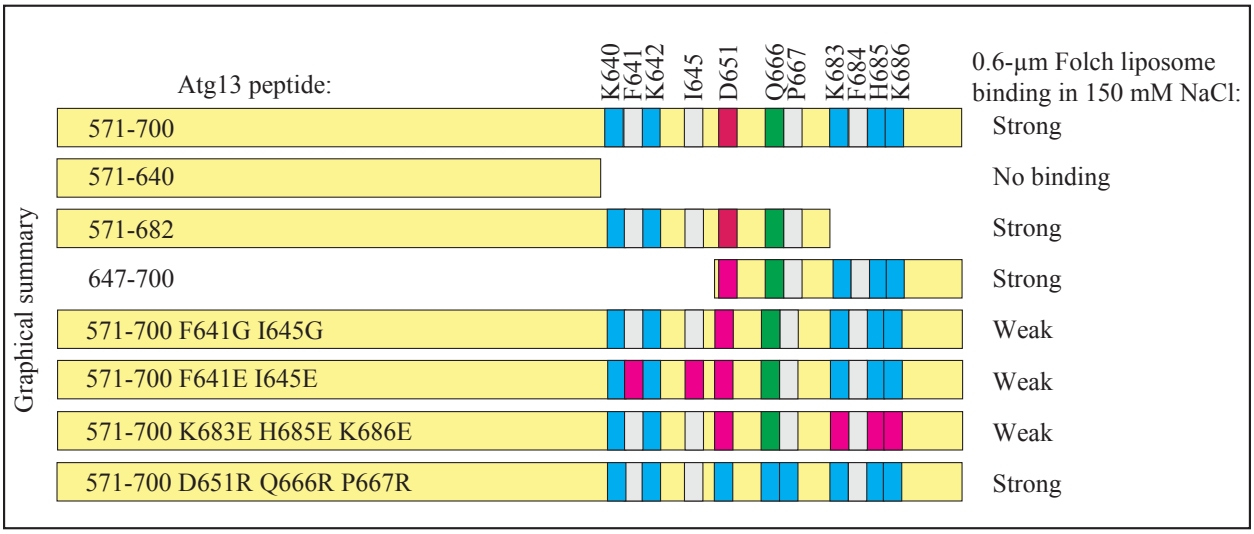

Figure S5. Graphical summary of truncation and mutagenesis data on binding of the Atg13 peptides to Folch liposomes at 150 mM NaCl. Motifs and residues in the sequence are color coded: peptide, maize; cationic residues, blue; anionic residues, magenta; hydrophobic residues, gray; polar residues, green. Related to Figure 2.

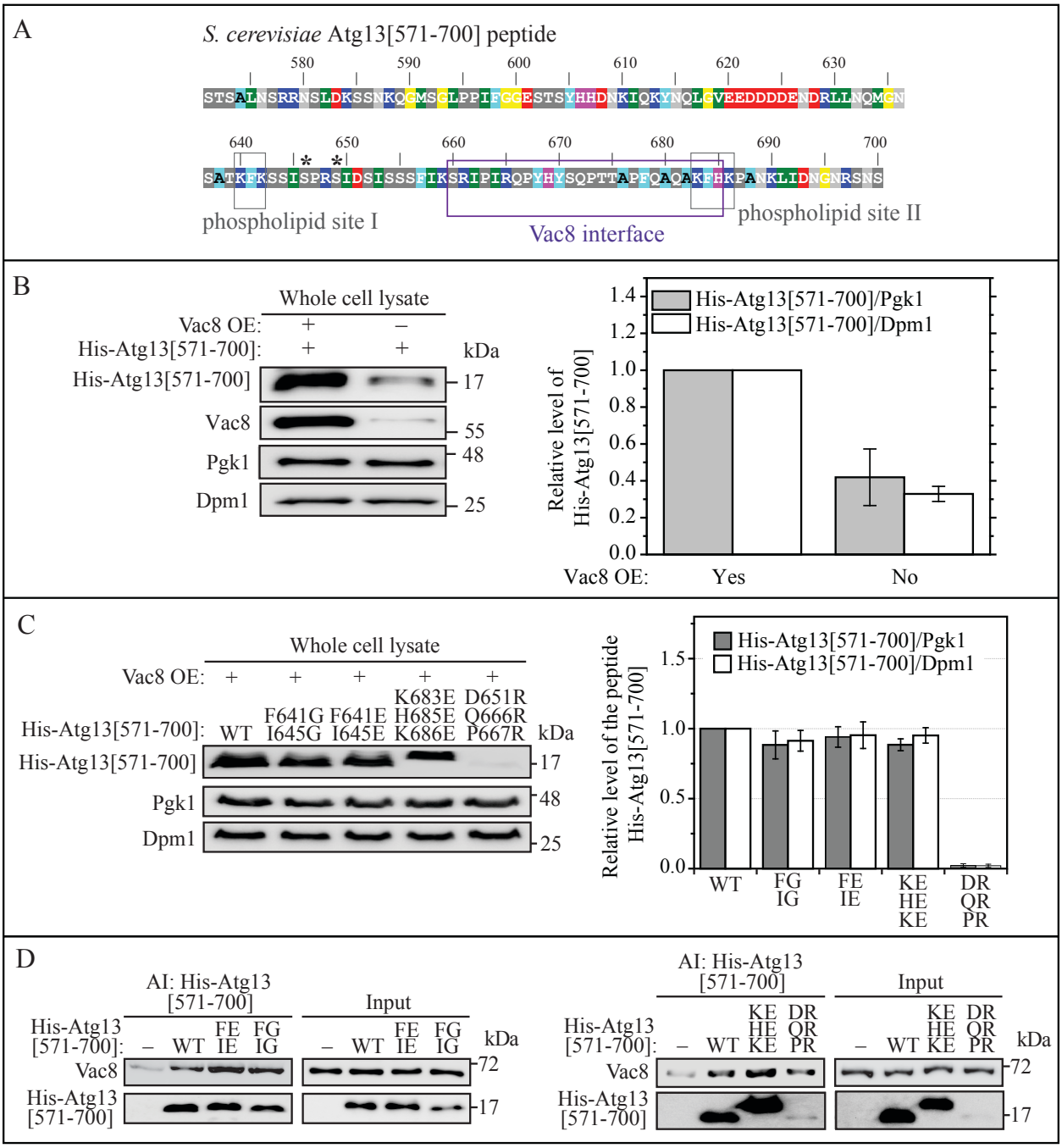

Figure S6. The interaction of Atg13[571-700] with Vac8 stabilizes the peptide in MKO cells. (**A**) Amino acid sequence of Atg13[571-700] created in the BioEdit Sequence Alignment Editor [33]. The phospholipid-binding motifs identified in this study are highlighted by gray rectangles. The Atg13 sequence forming the interface with Vac8 (Park et al, co-submitted manuscript) is highlighted by a purple rectangle. Asterisks mark Ser residues that are phosphorylated by TOR in nutrient-rich conditions. (**B, C**) Analysis of protein levels in the MKO cells. The plasmid pCuHis$_6$-Atg13[571-700]-Ss(424) was transformed into the MKO strain with or without the pVac8(426) plasmid overexpressing Vac8. MKO cells were cultured in nutrient-rich conditions to OD_{600} ~1 and then shifted to nitrogen starvation medium for 1 h. The lysates were TCA precipitated, and the proteins were separated by SDS-PAGE and detected with the indicated antibody or antisera. (D) His-tag affinity-isolation experiment. Other details are presented in the legend to Figure 3. Related to Figure 3.

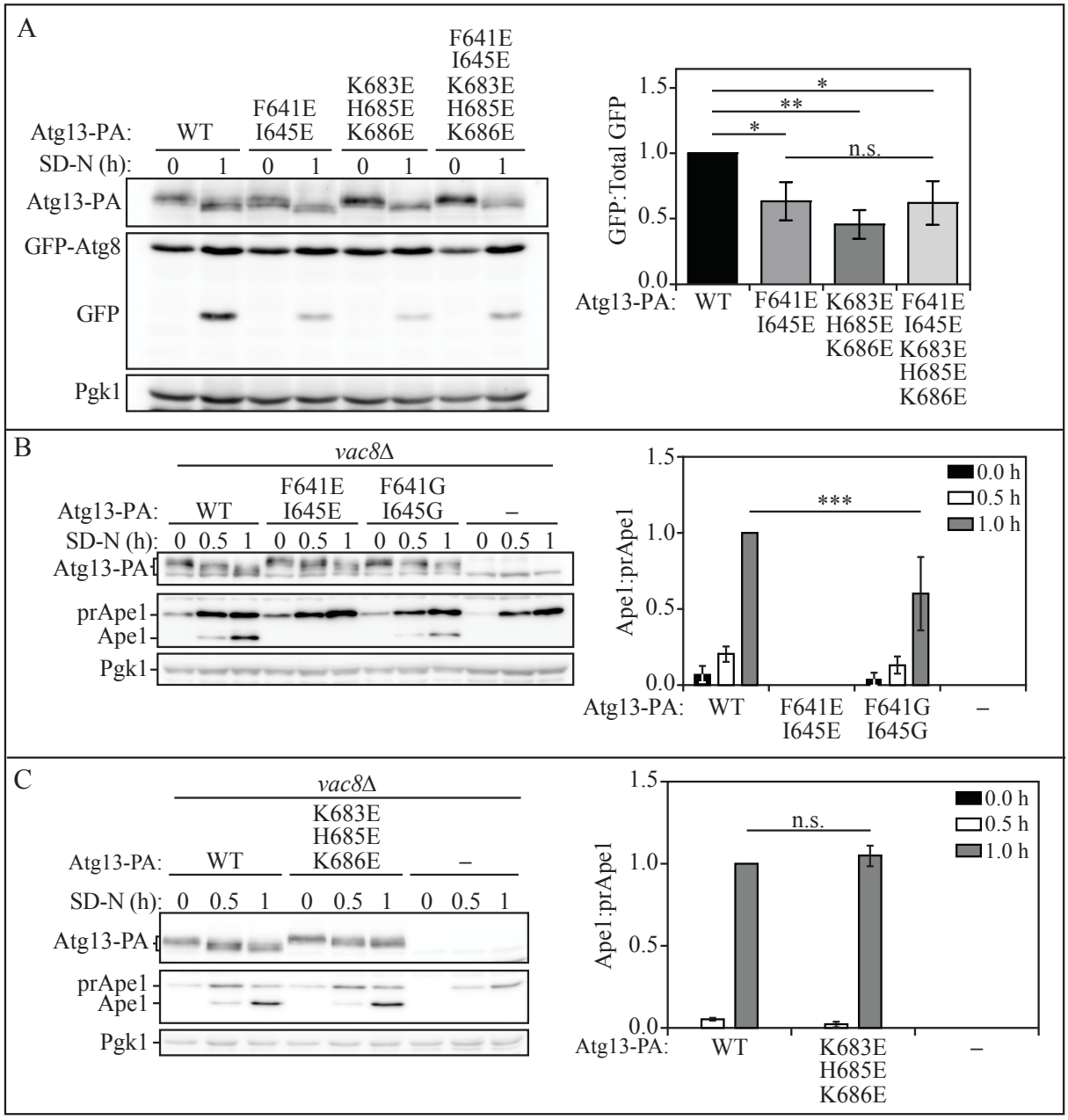

Figure S7. Autophagy activity of Atg13 mutants. (**A**) Autophagy activity was determined using the GFP-Atg8 processing assay in WT, Atg13^{F641,I645E}, Atg13^{K683,H685,K686E} and Atg13^{F641,I645,K683,H685,K686E} mutants under nutrient-rich conditions and after 1 h of nitrogen starvation. Error bars indicate the standard deviation of 3 independent experiments. Statistical analysis by ANOVA: * P <0.05; ** P <0.01; n.s., no significant difference. (**B**) Autophagy activity was measured with the prApe1 processing assay in *vac8*Δ deletion strains expressing either WT Atg13, Atg13^{F641,I645E}, or Atg13^{F641,I645G} mutants or deleted for *ATG13* under nutrient-rich conditions and after 0.5 and 1 h of nitrogen starvation. Error bars indicate the standard deviation of 3 independent experiments. Statistical analysis by ANOVA: *** P <0.001. **(C)** Autophagy activity was measured with the prApe1 processing assay in the *vac8*Δ strain expressing either WT Atg13, or the Atg13^{K683,H685,K686E} mutant or deleted for *ATG13* under nutrient-rich conditions and after 0.5 and 1 h of nitrogen starvation. Error bars indicate the standard deviation of 3 independent experiments. Statistical analysis by Student's t-test: n.s, no significant difference. Related to Figure 5.